Joint Radar Amplifier Circuit and Waveform Optimization for Ambiguity Function, Power-Added Efficiency, and Spectral Compliance

CASEY LATHAM, Student Member, IEEE
AUSTIN EGBERT, Student Member, IEEE
CHARLES BAYLIS, Senior Member, IEEE
Baylor University, Waco, USA

LAWRENCE COHEN, Senior Member, IEEE
Naval Research Laboratory, Washington, USA

ROBERT J. MARKS II, Fellow, IEEE
Baylor University, Waco, USA

Future radar transmitters must be adaptive and reconfigurable in real time to be able to share spectrum dynamically with wireless communications. We demonstrate the joint, back-and-forth optimization of the radar transmitter waveform and circuitry in a combined algorithm that can be used for real-time reconfiguration. While previously developed methods consider the waveform and circuit separately, resulting in emphasis on one of the criteria [ambiguity function (AF) or power efficiency], we show that the joint optimization of the circuit and waveform allows both the radar AF and circuit power-added efficiency (PAE) criteria to be gradually improved during the optimization. Measurement results are presented and analyzed to assess the convergence of the PAE and AF least-squares error, as compared to the AF template during an optimization under spectral mask and peak-to-average power ratio constraints.

Manuscript received February 28, 2018; revised August 30, 2018; released for publication November 12, 2018. Date of publication April 16, 2019; date of current version June 7, 2019.

DOI. No. 10.1109/TAES.2019.2909725

Refereeing of this contribution was handled by J. T. Curran.

This work was supported by the National Science Foundation under Grant ECCS-1343316.

Authors' addresses: C. Latham, A. Egbert, C. Baylis, and R. J. Marks II are with the Department of Electrical and Computer Engineering, Baylor University, Waco, TX 76798 USA, E-mail: (caseylatham@ieee.org; Austin_Egbert@baylor.edu; Charles_Baylis@Baylor.edu; Robert_Marks@baylor.edu); L. S. Cohen is with the Radar Division, Naval Research Laboratory, Washington, DC 20375 USA, E-mail: (lawrence.cohen@nrl.navy.mil). *(Corresponding author: Charles Baylis.)*

I. INTRODUCTION

Cognitive and adaptive radar transmitters must optimize for multiple priorities, including ambiguity-function (AF) performance of the amplifier's output waveform, power-added efficiency (PAE) of the transmitter power amplifier, and spectral mask compliance that may change based on surrounding wireless spectrum users. While significant progress has been made in the literature in the traditionally separate areas of radar waveform optimization and power amplifier circuit optimization, this paper demonstrates the joint optimization of both the waveform and the circuit to meet the following three goals:

1) AF performance;
2) PAE;
3) compliance with spectral regulations.

To our knowledge, this paper demonstrates the first successful joint circuit and waveform optimization for radar transmitters. PAE is defined by the following well-known equation:

$$\text{PAE} = \frac{P_{\text{out,RF}} - P_{\text{in,RF}}}{P_{\text{dc}}} \times 100\% \qquad (1)$$

where $P_{\text{in,RF}}$ and $P_{\text{out,RF}}$ are the input and output radio-frequency (RF) power, respectively, and P_{dc} is the dc power. The PAE is a metric describing the percentage of the dc power that is converted into additional RF power beyond that provided by the input RF signal.

Typically, efforts at radar waveform and circuit optimizations are performed independently, where the circuit is often optimized with no consideration of the waveform and vice versa. Gorji presents an iterative algorithm that adjusts the waveform parameters space-time adaptive weights to maximize the signal-to-interference-plus-noise ratio [1]. Consideration of the radar transmitter hardware's effect on a waveform optimization is introduced by Jakabosky [2]. Eustice performs radar waveform optimization using alternating projections for multiple constraints and objectives with a simple model used to represent the transmitter nonlinearities [3]. The feasibility of a reconfigurable radar is demonstrated through recent innovations in circuit optimization techniques [4], adaptive amplifier module construction [5], [6], and high-power tunable circuitry [7].

However, because the waveform affects the performance of the circuit and the circuit affects the performance of the waveform, it is expected that optimizing the nonlinear circuit and waveform together can improve the performance of both. In addition, joint optimization can provide gradual progress toward all objectives, rather than first achieving one goal and then attempting another, which often does not reach a solution that is a good compromise between all objectives. To our knowledge, this paper details the first complete algorithm for joint radar transmitter waveform and circuit optimization.

The function of a radar is to detect its target with desired range and Doppler resolution. The ambiguity in range and Doppler detection is represented by the AF, which was first derived by Woodward [9]. The AF is used to describe the output of the matched filter, based on the radar waveform $x(t)$, at displacements τ and u in range and Doppler, respectively, from the actual range and Doppler of the target under examination [10], [11].

$$\chi_x\ (\tau, u) = \int_{-\infty}^{\infty} x\,(t)\,x^*\,(t-\tau)\,e^{-j2\pi ut}dt. \qquad (2)$$

Eustice describes the AF and its derivation in more detail [11].

Waveform optimization techniques have been derived using the AF as a measure of the range and Doppler resolution performance achievable by the waveform. Wilcox presents a classic synthesis technique using a least-squares estimation approach to approximate a desired AF [12]. An extension of this work by Sussman allows functions without Hermitian symmetry and nonunity energy values [13]. Since real waveforms possess even magnitude spectra and odd phase spectra (Hermitian symmetry), the opening of the optimization to non-Hermitian waveforms allows complex waveforms to be used in the optimization. This, however, is reasonable, because the baseband waveform selected is upconverted onto a carrier frequency, which results in a real waveform from even a complex baseband waveform. Wolf considers AF synthesis using a pattern search with predetermined basis functions; however, only phase-modulated waveforms are considered [14]. Gladkova [15], [16] extends Wilcox's method to Hermite waveforms, which are often too difficult to generate [17], [18]. Costas focuses on obtaining an ideal "thumbtack" AF, with a sharp main lobe near the range/Doppler plane origin and no ambiguity elsewhere [19]. Patton has demonstrated joint optimization of the waveform and receiver signal processing to satisfy auto- and cross-correlation constraints [20], synthesis of a waveform based on its spectrum [21], and waveform optimization to satisfy autocorrelation and modulus requirements [22]. Kassab explores alternating projections for radar waveform synthesis based on the autocorrelation [23]. Blunt and Jakabosky demonstrate the implementation and optimization of polyphase-coded waveforms for radar [24], [25], and describe transmitter-in-the loop optimization for radar waveforms [2], [26].

Similarly, circuit optimization techniques have been developed that can be used for fast circuit tuning. Lu and Vaka-Heikkila discuss reconfigurable amplifiers using microelectrical mechanical systems switches [27], [28]. Deve describes a variable impedance matching network tunable between 1 and 3 GHz [29]. Sun describes the need for fast tuning with reconfigurable transmitters [30] and demonstrates real-time impedance matching for antennas using a genetic algorithm [31], [32]. Qiao demonstrates a real-time reconfigurable amplifier using a genetic algorithm [5]. While genetic algorithms have been used in some proposed real-time optimizations, Du Plessis discusses this approach and states that genetic algorithms tend to be slower than other algorithms in many applications [33]. Fellows [34] and Barkate [35] demonstrate modified gradient-based searches for power amplifiers. Bandler describes pattern and simplex searches as alternatives to the gradient search [36]. A simplex circuit search is demonstrated by Tsatsoulas [37], and Barkate compares pattern, simplex, and gradient searches in multidimensional circuit optimization, demonstrating that the gradient search approach is a very consistent approach for multidimensional optimization [38]. Gradient-based vector searches for radar power amplifiers have been demonstrated by Fellows [34], [4] and Barkate [35] allowing amplifier load-impedance optimization to maximize PAE while meeting requirements on adjacent-channel power ratio. Hays demonstrates the use of a varactor tuning network for fast reconfiguration designed for amplifier applications [39].

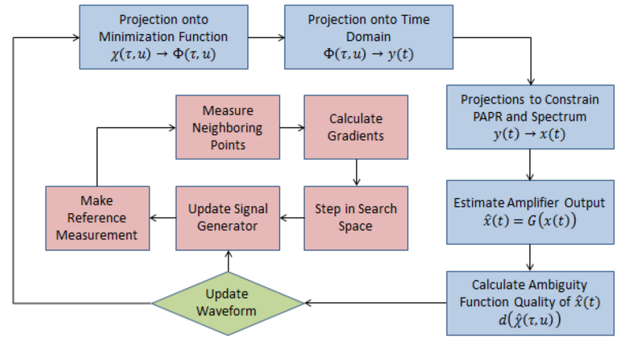

Fig. 1. Joint circuit and waveform optimization flow diagram.

The impact of a nonlinear power amplifier on the radar waveform's AF is documented by Eustice [40]. In addition, the waveform's impact on circuit performance is evident based on the well-known relationships between peak-to-average power ratio (PAPR) and both efficiency and linearity for a given amplifier. These issues of intertwining impact make a joint circuit and waveform optimization approach very attractive. The need to provide a joint circuit and waveform optimization is presented by Baylis [41].

The present paper brings together the circuit and waveform optimizations and allows them to be performed in a back-and-forth manner. In transmission using nonlinear power amplifiers, the back-and-forth approach to circuit and waveform optimization is expected, in many cases, to provide a better overall solution than the individual optimization of the circuit followed by the individual optimization of the waveform (or vice versa). This is related to the general inability to apply the principle of superposition to nonlinear situations.

Section II describes the joint circuit and waveform optimization. Section III details the measurement setup. Section IV shows the measured results and how joint and sequential (circuit-then-waveform) optimizations compare. Section V provides conclusions and ideas for future work.

II. CIRCUIT AND WAVEFORM OPTIMIZATION OVERVIEW

Fig. 1 illustrates the joint circuit and waveform optimization. The outer loop, containing boxes shaded in blue, is the Eustice alternating-projections waveform optimization [3]. The inner loop, containing boxes shaded in red, is a

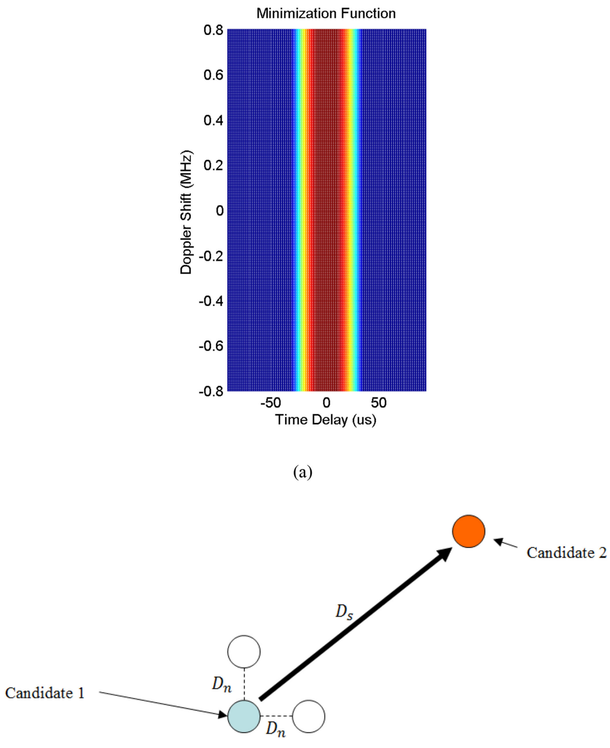

(a)

(b)

Fig. 2. (a) Ambiguity function minimization template showing areas of allowed ambiguity (red) and areas for ambiguity minimization (blue). (b) Gradient circuit optimization, using neighboring points at Candidate 1 to estimate the gradient, and taking a step of size D_s in the gradient direction to obtain Candidate 2 [8].

modified gradient-based circuit optimization adapted from Fellows [4]. The circuit is updated with the best performing waveform after every five waveform iterations. The timing of the optimization is that five waveform optimization iterations are performed, followed by a circuit optimization with the best performing waveform. This procedure then repeats until the optimization is halted.

We consider the following three goals for the overall optimization:

1) desired range/Doppler AF performance;
2) PAE maximization;
3) spectral compliance.

In the Eustice method of alternating projections waveform optimization (the outer loop in Fig. 1), the waveform is projected onto three sets [3]. The first set, called the minimization function, is shown in Fig. 2(a). The areas in blue are the range/Doppler combinations to be minimized. The minimization areas are given different levels of importance, as demonstrated through proceeding from dark blue to yellow in Fig. 2(a). The waveform is then projected onto a set of all waveforms that meet the peak-to-average-power ratio requirement. Last, the waveform is projected onto the set of spectrally compliant waveforms. Spectral mask compliance is determined by the value of the metric S_m [4]:

$$S_m = \max(s - m) \tag{3}$$

where s is the value of the measured spectrum in dBm and m is the value of the mask in dBm.

If $S_m \leq 0$, the spectrum is in compliance (below or at the mask), and if $S_m > 0$, the spectrum is out of compliance (spectrum above the mask). The final projection onto the set of functions meeting the spectral mask criteria essentially uses the mask as a bandpass filter.

For the circuit optimization, in which the load reflection coefficient Γ_L of the amplifier is adjusted using an automated tuner with a controller, the approach of Fellows [4] is modified in that the spectral mask is not considered in the circuit optimization, because it is included in the waveform part of the optimization. The resulting algorithm is an unconstrained optimization of PAE, similar to the output power optimization previously presented by Baylis [8]. A gradient search is used in the Smith Chart to maximize the PAE [Fig. 2(b)], using two neighboring points at the first candidate Γ_L to estimate the PAE gradient, then locating the next candidate Γ_L a distance D_s from the first in the direction of the gradient. The process repeats until the candidate Γ_L has a lower PAE than the previous candidate. At this point, the algorithm divides the current step size in half. This process continues until D_s is reduced below a certain threshold, resulting in maximum PAE [8].

As mentioned, the optimization sequence consists of five waveform optimizations, followed by a circuit optimization that uses the best available waveform, based on least-squares comparison to the AF template and spectral mask compliance. While the reverse process could be workable (the waveform could be updated with the best circuit setting every five circuit iterations), the results would likely take much longer to achieve, and potentially change significantly through the search. The best circuit setting heavily depends upon the best waveform, because the AF template significantly affects the closeness of the waveform to violation of spectral mask limitations. As such, it is best to ensure the waveform optimization moves along quickly in comparison with the circuit optimizations, to allow a near-final waveform to be achieved quickly. Additionally, a circuit optimization step takes significantly more time than a waveform optimization step, due to the time required for actuation and movement of the impedance tuner.

III. MEASUREMENT SETUP

The optimizations were run on a test bench setup controlled by MATLAB, which controls a Maury Microwave load pull tuner and a Keysight Technologies signal generator. Our measurement setup for demonstration of impedance tuning algorithms is shown in Fig. 3. For the initial experiments described in this paper, the Maury tuner was used in place of an actual reconfigurable circuit to demonstrate the effect of adapting the load impedance using search algorithms. The developments presented in this paper will be later investigated in reconfigurable amplifiers for real-time performance. Measurements are read from a Keysight Technologies signal analyzer and power sensor. The optimizations were measurement-tested on two different

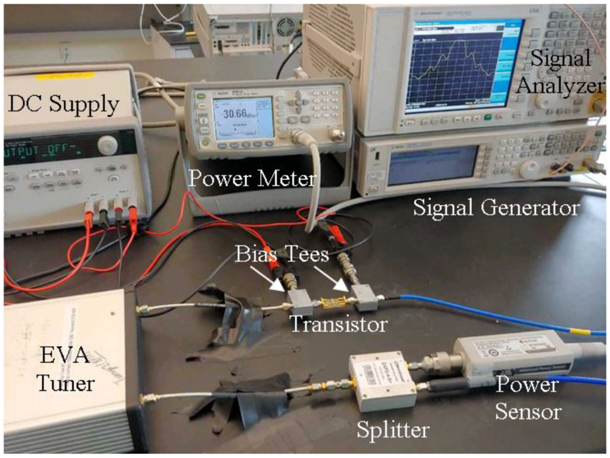

Fig. 3. Measurement setup (Maury mechanical tuner is used in place of "EVA Tuner" for this work).

amplifier devices: a Microwave Technologies (MWT) High Gain GaAs FET and a Skyworks InGaP packaged amplifier. The optimizations were performed from starting Γ_L values that were varied to include points from all around the Smith Chart, to ensure that various linearity regions were examined. For both joint and sequential optimizations, the initial baseband waveform upconverted to 3.3 GHz for the optimization was a modified two-tone waveform given by

$$x(t) = \frac{1}{2} e^{j\omega t} + e^{-j\omega t}. \quad (4)$$

After the initialization, five iterations of simulated waveform optimization were performed using the controlling computer. Sequential optimization first performs the entire circuit optimization using the approach of Baylis [8], where the gradient-based approach is used to find the load reflection coefficient (Γ_L) that results in the maximal PAE. At this point, the Γ_L is fixed and the waveform optimization of Eustice [3] takes over. A complete waveform optimization is completed, which is a total of 40 waveform iterations, including the first five simulated waveforms.

Joint optimization operates differently than sequential optimization. Instead of doing circuit optimization followed by waveform optimization, the two optimizations are performed in an alternating manner (five waveform iterations followed by one circuit optimization) to approximate parallel circuit and waveform optimization. As in the case of sequential optimization, the process begins with five simulated waveform iterations. The measurement optimization begins with five waveform iterations, then the circuit optimization uses the waveform with the lowest least-squares distance to perform the circuit optimization. The next five waveform optimization iterations are then performed. This process continues until a total of 40 waveform iterations have been completed (including simulated and measured waveforms). After 40 waveform iterations have been performed, the circuit search runs until convergence. From the final Γ_L, five additional waveform optimizations are performed, allowing the final waveform to be optimized for the final value of Γ_L.

In presenting plots of the optimization versus iterations, the unit of "equivalent waveform iterations" is used. It is reasonably anticipated that a measurement-based circuit optimization iteration will require approximately five times as much time as a circuit optimization, due to the time it takes to move the tuners to a new Γ_L value. Therefore, in comparing performance between joint and sequential operations, this approximate timing is used. Each circuit iteration is approximated to require the same time five equivalent waveform iterations for comparison of performance evolution in these diagrams.

A range radar minimization function was used for these experiments, minimizing the ambiguity everywhere in the range/Doppler plane except for along the Doppler axis [Fig. 2(a)]. With a range radar, the waveform optimization yields a short pulse in the time domain, which corresponds to a near constant in the frequency domain. However, since the spectral mask does not allow this, the optimization is forced to select a waveform that is as close as possible to the range radar minimization function while meeting spectral requirements. The PAPR limit is often approached as well by the pulse-like time domain waveforms producing good range resolution. This, in turn, results in lower PAE.

It is the transmitter amplifier *output* waveform that should be examined in a radar waveform optimization. An input waveform is synthesized that is expected to produce the desired output waveform, based on a simple model for amplifier nonlinearities. This model is used to provide the input waveform that, given the amplifier nonlinearities, can produce the desired output waveform. For purposes of this initial work, a simple hyperbolic tangent model is used to model the input–output voltage response of the amplifier [11]. The model is defined as follows:

$$v_{\text{out}} = a \tanh(\beta v_{\text{in}}). \quad (5)$$

The model coefficients a and β are found by fitting (5) to a measured input–output characteristic, as shown in Fig. 4. Note that this model may not be completely sufficient to account for all nonlinearities, including amplitude-modulation to phase-modulation distortion and memory effects. Since the model cannot account for all nonlinearities, the model is limited for highly nonlinear amplifiers. The model has limited performance for waveforms with low duty cycles, such as a time-domain impulse function, since the waveform would mostly map onto the flat tails of the hyperbolic tangent model. A more complex amplifier model could be inserted into this approach to obtain even better results.

IV. MEASUREMENT RESULTS

Traditional methods of finding the maximum-PAE Γ_L can require a significant number of measurements. The full load-pull measurement using the Maury Microwave load-pull tuner shown in Fig. 5 requires 292 measurements, for example. This full load-pull measurement provides a good

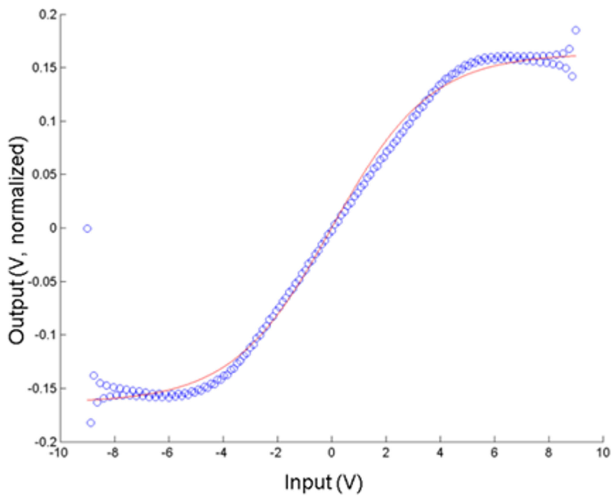

Fig. 4. Measured input–output data (blue circles) and model simulation results (red line). This nonlinearity model allows for input waveform synthesis based on a desired output waveform.

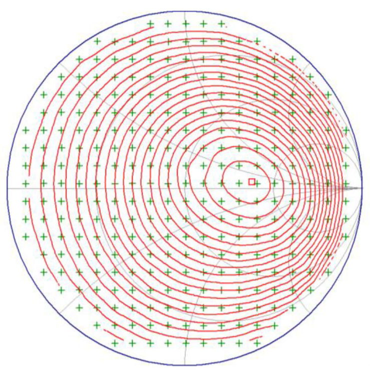

(a)

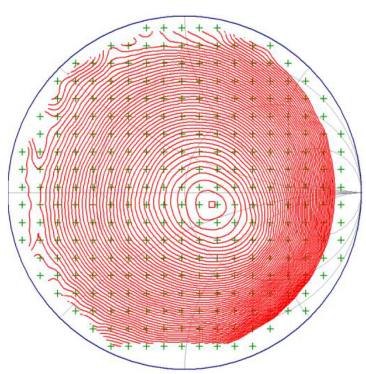

(b)

Fig. 5. PAE load-pull comparison. (a) Load-pull for the MWT amplifier, showing the maximum PAE point, indicated by the red square. (b) Load-pull for the Skyworks amplifier, showing the maximum PAE point, indicated by the red square.

point of comparison for circuit optimization to demonstrate the accuracy of the searches, as both the load pull and circuit optimization find the Γ_L with maximum PAE for a given fixed waveform. The circuit optimization, however, does so with far fewer measurements. The traditional load-pull measurement results for the MWT amplifier are

TABLE I
Comparison of Joint and Sequential Optimizations

Opt. Type	Amplifier	PAE (%)	S_m (dB)	WF LS Dist.	Mean End Γ_L	End Γ_L σ
Seq.	MWT	0.314	1.570	0.099	0.17/-29.38°	0.035
Joint	MWT	2.205	2.437	0.100	0.07/126.57°	0.057
Seq.	SKY	2.548	-3.044	0.105	0.40/7.96°	0.052
Joint	SKY	2.776	-0.256	0.105	0.42/-17.76°	0.049

shown in Fig. 5(a) for a modified chirp waveform. The PAE maximum for the MWT amplifier is shown by the red square, which is located at $0.17/-23.99°$. The load-pull measurement results for the Skyworks amplifier are shown in Fig. 5(b). The PAE maximum for the Skyworks amplifier is also shown by the red square, which is located at $0.38/5.14°$. The load pull measurements, as well as the circuit optimization part of sequential optimization, were performed with the same waveform, in order to maintain consistency between all optimizations.

Table I shows the average results for both joint and sequential (circuit first, then waveform) optimization using both the MWT and the Skyworks (SKY) devices. On average, joint optimization results in a higher PAE than sequential optimization. This is because joint optimization is able to take advantage of the tradeoff that exists between the circuit and the waveform. The standard deviation (σ) of Γ_L, based on the error vector from the complex mean Γ_L, is reasonable for all of the measurements. For all of the results listed in Table I, the PAE is extremely low. This is not due to an issue with the circuit optimization, as the circuit optimization is able to achieve a PAE of 30% for the MWT amplifier and 11% for the Skyworks amplifier, both of which are the expected maximum for the respective amplifiers. When the circuit optimization is able to reach a high PAE, this is because the waveform has a duty cycle of 100%. When the range radar minimization function is used, the duty cycle is very low, around 10–15%. While a small duty cycle is beneficial for range detection, it causes a significant drop in PAE.

Even though the starting exponential waveform has a duty cycle of 100%, the final waveform does not. The given ambiguity minimization function tends to cause very short-burst waveforms for good range detection, leading to a waveform that typically has a duty cycle of 10 to 15%. Since the PAE is calculated over one whole period, the substantial amount of OFF time decreases PAE because the dc bias power is still being used. To increase efficiency in practice, the bias power can be turned OFF during the waveform "OFF" times once the optimization has settled in on a repeatable waveform. This can be performed using envelope tracking techniques, for example. This will boost the efficiency by the factor of duty-cycle decrease, but is not performed in the experiments detailed in this paper.

Table I also shows the spectral mask compliance, indicated by the metric S_m. For the MWT amplifier, the average end S_m is greater than 0, indicating that most of the time, the final waveform is not spectrally complaint. For the

Skyworks amplifier, the average S_m is less than 0, indicating that most of the time, the waveform is spectrally compliant. It is suspected that the lack of spectral compliance for the MWT amplifier is due to inadequacy with the nonlinearity model. While the nonlinearity model seems to provide reasonably good output-waveform performance for waveforms with high duty cycles, it seems to be less accurate in predicting results for waveforms with low duty cycles, such as the range radar waveform resulting from this optimization. In addition, the MWT amplifier seems to be driven further into compression than the Skyworks amplifier, requiring more complex modeling techniques not available from the simple model of (5).

The waveform least-squares distance from the ambiguity minimization function is also shown in Table I. A least-squares distance of 1.0 would indicate that the AF did not look anything like the minimization function. A least squares distance of 0.0 would indicate that the AF looked exactly like the minimization function. As shown in Table I, both joint and sequential optimizations produce a waveform that matches the AF template well. Since both optimizations perform approximately the same number of waveform iterations, a similar least squares distance is expected.

Table I also shows the average final reflection coefficient (Γ_L) for both sequential and joint optimizations. For the MWT amplifier, the average distance between the end Γ_L and the maximal PAE Γ_L from the load pull is 0.016 for sequential optimization and 0.236 for joint optimization. For the Skyworks amplifier, the average distance between the end Γ_L and the maximal PAE Γ_L from the load pull is 0.0296 for sequential optimization and 0.1630 for joint optimization. This demonstrates the impact that the waveform used for the circuit optimization has on the final Γ_L. Sequential optimization, which uses the starting exponential for the circuit optimization, results in a final Γ_L that is very close to the maximal Γ_L found by the load pull. Joint optimization, on the other hand, ends with a Γ_L that is not very close to the load pull's maximal Γ_L, when using the initial waveform for the measurement. This is because joint optimization takes advantage of the tradeoff between the circuit and the waveform, as the waveform used for each circuit step changes as the optimization continues. This allows the waveform and circuit to become intertwined, allowing the optimization to perform better, resulting in higher PAE. This also allows for more on-the-fly optimization, where the parameters can be changed periodically without having to start the optimization from the beginning.

While Table I allows for comparison of the end result of the optimizations, it is the ability of the intermediate states in the optimization to provide a good compromise between PAE and waveform performance that demonstrates the true value of joint optimization. A comparison of the least squares distance for joint and sequential optimizations versus equivalent waveform iterations is shown in Fig. 6. The PAE values for joint and sequential optimizations are compared in Fig. 7. The spectral mask compliance metric S_m is shown versus equivalent waveform iteration in

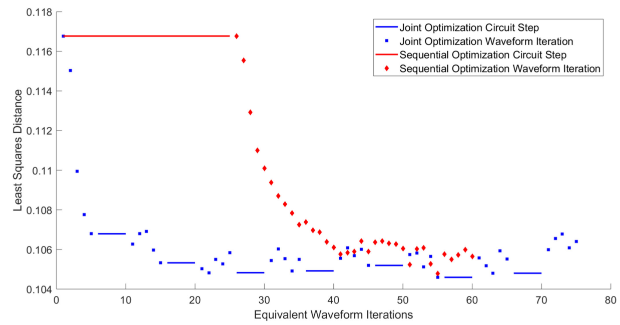

Fig. 6. Comparison of least-squares distances between the actual waveform ambiguity function and the ambiguity function template for joint (blue) and sequential (red) optimizations for the Skyworks amplifier with starting $\Gamma_L = 0.8\underline{/-90^\circ}$.

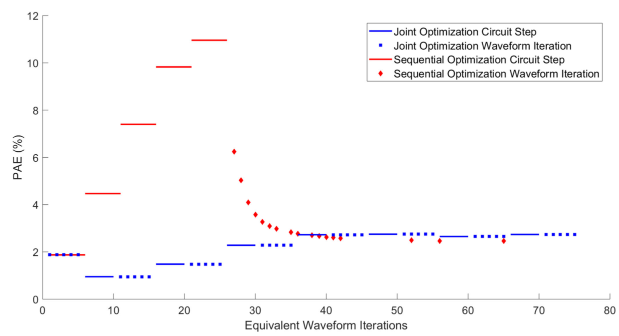

Fig. 7. Comparison of PAE for joint (blue) and sequential (red) optimizations for the Skyworks amplifier with starting $\boldsymbol{\Gamma_L} = 0.8\underline{/-90^\circ}$.

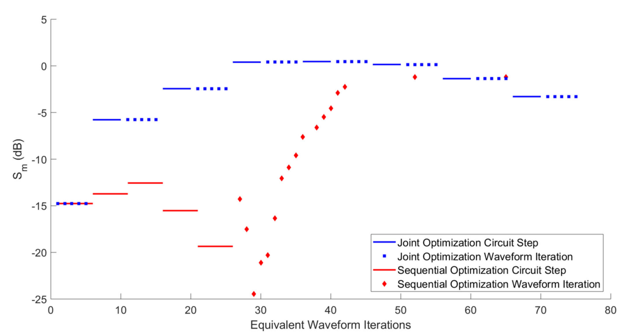

Fig. 8. Comparison of $\boldsymbol{S_m}$ for joint (blue) and sequential (red) optimizations for the Skyworks amplifier with starting $\boldsymbol{\Gamma_L} = 0.8\underline{/-90^\circ}$.

Fig. 8. Joint optimization is shown in blue and sequential optimization is shown in red. Circuit steps are shown by lines covering five equivalent waveform iterations due to the anticipated time required (as previously explained), while waveform optimization is shown by blue squares for joint optimization and red diamonds for sequential optimization. For the circuit steps in joint optimization, the least-squares distance shown is the least-squares distance measured at the initial value of Γ_L from which the circuit optimization was taken (some fluctuations in the least squares distance can be expected as Γ_L moves around the Smith Chart, but measurements were not performed to assess these fluctuations).

When examining sequential optimization, the circuit optimization took 25 equivalent waveform iterations to

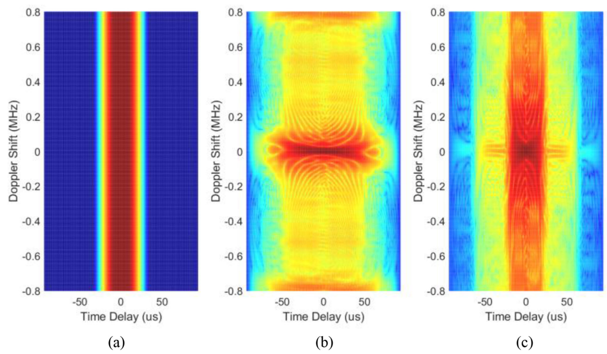

Fig. 9. Ambiguity function comparison at equivalent waveform iteration 26 including (a) ambiguity function minimization template, (b) ambiguity function from sequential optimization, and (c) ambiguity function from joint optimization.

complete, which is equivalent to five circuit steps. These circuit steps were taken using the starting exponential waveform, which has a least squares distance of 0.1168. After the circuit optimization converged at iteration 25, waveform optimization was performed from the final Γ_L. Five waveform iterations were then performed in a complete simulation environment. The algorithm then performed 35 waveform optimization iterations on the measurement setup. After a total of 60 equivalent waveform iterations, the sequential optimization was completed.

For joint optimization, the circuit and waveform optimizations are completed in a back-and-forth approach. The first five waveforms, not shown in the plots, were completed in a simulation environment, as in the case of the sequential optimization. Next, beginning with equivalent waveform iteration 1, five waveform iterations were completed on the measurement setup. At this point, a circuit step was taken using the waveform with the lowest least squares distance from the previous five waveform iterations. Because the waveform changes as the Γ_L value is changing, joint optimization takes slightly longer to complete. Both the joint and sequential optimization converge to similar PAE values, with joint optimization producing a slightly higher end PAE value due to the Γ_L value being a tradeoff between the circuit and waveform.

The strength of joint optimization comes from how quickly it is able to produce a usable result. In integrating with a cognitive radar optimization, it may be necessary to operate successfully without having the full time to complete an optimization. Since joint optimization immediately starts improving the waveform, the waveform is usable much earlier than with sequential optimization. As shown in Fig. 6, by equivalent waveform iteration 26, joint optimization has found a waveform that is usable and is much better than sequential optimization. A comparison of the AF from sequential and joint optimizations with the minimization function is shown in Fig. 9. The joint optimization AF [Fig. 9(c)], looks much like the range template of Fig. 9(a), with the ambiguity aligned along the Doppler axis. The sequential optimization ambiguity function actually aligns much of its ambiguity along the range axis, preventing high-resolution range detection at this stage of the optimization.

Fig. 7 shows that for sequential optimization, circuit optimization continues to increase the PAE with a nonrange waveform until it reaches the maximum, which is around 11%. This is close to the maximum PAE that the Skyworks amplifier is able to achieve. After five circuit steps, the search converges, and the waveform optimization begins. For the waveform optimization, the PAE immediately starts decreasing. This is because the range radar template results in an optimized waveform with a low duty cycle (approximately 10%). This therefore decreases the efficiency of the waveform, as the waveform is instead being limited by the peak-to-average-power ratio, which is used as a constraint in the waveform optimization to maintain useful PAE. In addition, since the waveform optimization does not attempt to improve the PAE, these measurements were not originally coded to be read from the test setup during waveform optimization. Instead, the PAE and S_m values were read whenever a waveform produced a lower (better) least squares distance.

Joint optimization again takes slightly longer to complete than sequential optimization. Since joint optimization begins with waveform optimization at the starting Γ_L, the first five nonsimulated waveform iterations are shown with the initial PAE at the starting Γ_L. Even though in reality the PAE will be affected by the change in waveform, it is not remeasured until a circuit optimization iteration is performed. After the first five measured waveform iterations, a circuit optimization is performed to calculate the next Γ_L to be used. Once the circuit has been adjusted to move the Γ_L value, five more waveform optimization iterations are performed at this Γ_L point.

As the joint optimization continues, the PAE continues to increase until equivalent waveform iteration 35, where the values begin to peak. From this point, the waveform continues to be optimized, leading to waveforms that better meet all parameters. By the end of the search, joint optimization yields a higher PAE value that demonstrates a good tradeoff between circuit and waveform parameters, with the final Γ_L for joint optimization differing from the final Γ_L position for sequential optimization. After the circuit optimization converges, five additional waveform iterations are performed to fine tune the waveform at the final Γ_L value, which, in this case, results a small increase in the PAE.

The unfolding of spectral compliance versus equivalent waveform iteration is shown in Fig. 8. Sequential optimization starts with circuit optimization. Since the starting waveform has a narrow bandwidth, it results in high PAE and low S_m. As such, the spectrum is much further from its mask (lower S_m) for the initial sequential optimization iterations than for the joint optimization. As the circuit optimization works toward the maximal PAE point, the S_m values fluctuate, first increasing and then decreasing. This is due to changes in the linearity contours as the circuit optimization moves around the Smith Chart. Once the waveform optimization starts, the S_m values get closer to 0, as the AF gets closer to the range radar minimization template,

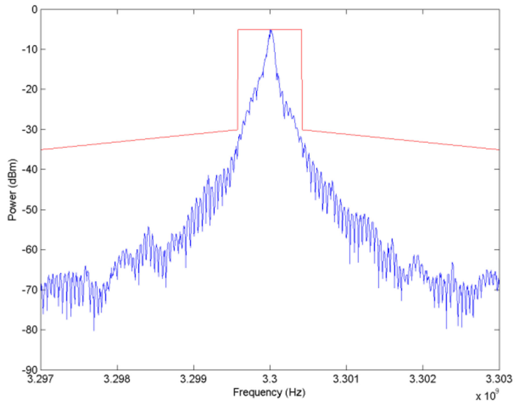

(a)

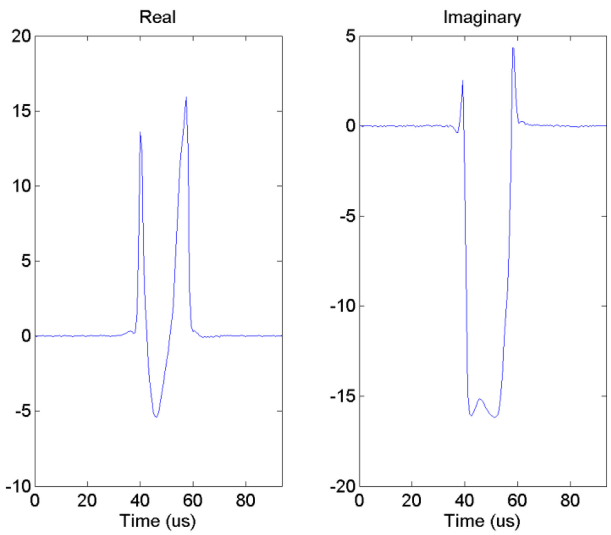

(b)

Fig. 10. Final waveform resulting from joint optimization of Skyworks amplifier. (a) Final spectrum. (b) Real and imaginary parts of the baseband time-domain waveform.

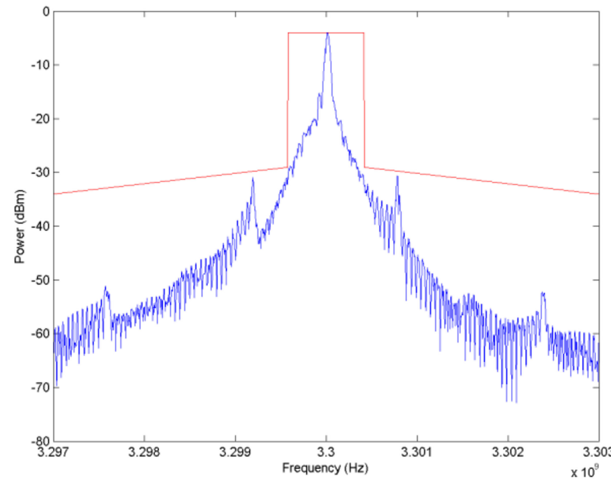

(a)

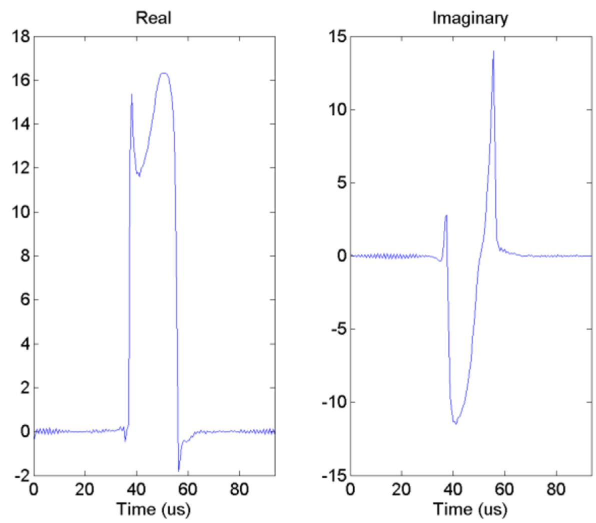

(b)

Fig. 11. Final waveform resulting from sequential optimization of Skyworks amplifier. (a) Final spectrum. (b) Real and imaginary parts of the baseband time-domain waveform.

resulting in a spectrum that is pressed against the mask. Again, the S_m value during the waveform optimization is measured whenever a waveform with a lower least squares distance is recorded. As shown in the graph, the optimization never goes above 0, meaning that the optimization is always spectrally compliant.

Unlike sequential optimization, joint optimization starts with a set of waveform iterations. As with PAE, the same S_m value is plotted for all of these points. Once joint optimization starts taking circuit steps, the S_m value starts to increase substantially, as the waveform optimization handles spectral compliance throughout the optimization and since each circuit step is taken with a waveform that pushes the spectral mask. By equivalent waveform iteration 15, joint optimization is already really close to pushing the spectral mask, a result of the waveform becoming wide bandwidth for good range resolution. As the optimization continues, though, joint optimization goes just out of spectral compliance ($S_m > 0$), due to inaccuracies and limitations of the real-time extracted nonlinearity model for the transistor. However, how close the predistortion model is to the limit illustrates just how much the optimization pushes the spectral mask. Despite the issues with the predistortion model, the measured amplifier output waveform is seen to be spectrally compliant ($S_m \leq 0$) after equivalent waveform iteration 56.

The final waveforms for joint and sequential optimization for the Skyworks amplifier (from the searches shown in Figs. 6–8) are shown in Figs. 10 and 11, respectively. In both cases, the equivalent baseband waveform is a short burst in the time domain, an attribute expected of a range-radar waveform. This results in a spectrum that is close to the mask constraints, as seen for both the joint (Fig. 10) and sequential (Fig. 11) searches.

V. CONCLUSION

A joint circuit and waveform optimization has been explored and is seen to produce useful results quicker than sequential optimization in which the amplifier load reflection coefficient is first completely optimized, followed by the waveform. Measurement results show that both joint and sequential optimizations produce waveforms with a similar least squares distance, while joint optimization yields a slightly higher PAE on average. The true usefulness of the joint optimization approach is based on the fact that the circuit and waveform alternatingly change slightly, allowing both a useful radar waveform for the given AF template and reasonable PAE to be simultaneously obtained more quickly than in a sequential optimization where the circuit and waveform are individually completely optimized. Because next-generation radars will operate in dynamic environments, various parameters—including operating frequency, bandwidth, and power—will change in real time. Thus, a real-time back-and-forth optimization will help to adjust parameters without the need to restart an optimization from the beginning. Additionally, if mechanically actuated reconfigurable circuits, such as those presented by Semnani [7], are used in the optimization, the reconfiguration time will likely exceed the pulse repetition interval and perhaps even the coherent processing interval of a radar. As such, the radar must be able to perform high-resolution detection while the joint optimization is performing. The demonstrated ability to get reasonable performance in all three criteria—AF, PAE, and spectral-mask compliance—during the joint optimization, as opposed to a situation where only one or two of these criteria perform well in a traditional sequential optimization, is critical to avoiding the need for radar "down time" while the circuit and waveform are reoptimizing.

ACKNOWLEDGMENT

The authors are grateful to E. Mokole for his helpful ideas concerning this work.

REFERENCES

[1] A. A. Gorji, R. J. Riddolls, M. Ravan, and R. S. Adve
Joint waveform optimization and adaptive processing for random phase radar signals
IEEE Trans. Aerosp. Electron. Syst., vol. 51, no. 4, pp. 2627–2640, Oct. 2015.

[2] J. Jakabosky, L. Ryan, and S. Blunt
Transmitter-in-the-loop optimization of distorted OFDM radar emissions
In *Proc. IEEE Radar Conf.*, Ottawa, ON, Canada, Apr./May 2013, pp. 1–5.

[3] D. Eustice, C. Latham, C. Baylis, R. J. Marks II, and L. Cohen
Amplifier-in-the-loop adaptive radar waveform synthesis,
IEEE Trans. Aerosp. Electron. Syst., vol. 53, no. 2, pp. 826–836, Apr. 2017.

[4] M. Fellows, C. Baylis, L. Cohen, and R. J. Marks
Real-time load impedance optimization for radar spectral mask compliance and power efficiency
IEEE Trans. Aerosp. Electron. Syst., vol. 51, no. 1, pp. 591–599, Jan. 2015.

[5] D. Qiao, R. Molfino, and S. M. Lardizabal
An intelligently controlled RF power amplifier with a reconfigurable MEMS-varactor tuner,
IEEE Trans. Microw. Theory Techn., vol. 53, no. 3, pp. 1089–1095, Mar. 2005.

[6] N. Kingsley and J. R. Guerci
Adaptive amplifier module technique to support cognitive RF architectures
In *Proc. IEEE Radar Conf.*, Cincinnati, OH, USA, May 2014, pp. 1329–1332.

[7] A. Semnani, M. Abu Khater, Y.-C. Wu, and D. Peroulis
An electronically-tunable high-power impedance tuner with integrated closed-loop control
IEEE Microw. Wireless Compon. Lett., vol. 27, no. 8, pp. 754–756, Aug. 2017.

[8] C. Baylis, L. Dunleavy, S. Lardizabal, R. J. Marks II, and A. Rodriguez
Efficient optimization using experimental queries: A peak-search algorithm for efficient load-pull measurements
J. Adv. Comput. Intell. Intell. Inform., vol. 15, no. 1, pp. 13–20, Jan. 2011.

[9] P. M. Woodward
Probability, Information Theory and Radar. New York, NY, USA: Pergamon, 1953.

[10] M. Cheney
A mathematical tutorial on synthetic aperture radar
SIAM Rev., vol. 43, no. 2, pp. 301–312, 2001.

[11] Eustice, D., Baylis, C., and Marks II, R. J.
Woodward's ambiguity function: From foundations to applications
In *Proc. Texas Symp. Wireless Microw. Circuits Syst.*, Waco, TX, USA, Apr. 2015, pp. 1–17.

[12] C. H. Wilcox
The synthesis problem for radar ambiguity functions
Math. Res. Center, Univ. Wisconsin, Madison, WI, USA, Tech. Summary Rep. 157, 1960.

[13] S. M. Sussman
Least-square synthesis of radar ambiguity functions
IRE Trans. Inf. Theory, vol. 8, pp. 246–254, 1962.

[14] J. D. Wolf, G. M. Lee, and C. E. Suyo
Radar waveform synthesis by mean-square optimization techniques
IEEE Trans. Aerosp. Electron. Syst., vol. AES-5, no. 4, pp. 611–619, Jul. 1969.

[15] I. Gladkova and D. Chebanov
On a new extension of Wilcox's method
WSEAS Trans. Math., vol. 3, no. 1, pp. 244–249, 2004.

[16] Gladkova, I. and Chebanov, D.
On the synthesis problem for a waveform having a nearly ideal ambiguity surface
In *Proc. Int. Conf. Radar Syst.*, Philadelphia, PA, USA, 2004.

[17] M. A. Sebt, A. Sheikhi, and M. M. Nayebi
Orthogonal frequency-division multiplexing radar signal design with optimised ambiguity function and low peak-to-average power ratio
IET Radar, Sonar Navig., vol. 3, no. 2, pp. 122–132, 2008.

[18] J. A. G. O. Byrnes
Computational Noncommutative Algebra and Applications: Proceedings of the NATO Advanced Study Institute on Computational Noncommutative Algebra and Applications. Berlin, Germany: Springer Science & Business Media, 2006, p. 351.

[19] J. P. Costas
A study of a class of detection waveforms having nearly ideal range—Doppler ambiguity properties
Proc. IEEE, vol. 72, no. 8, pp. 996–1009, Aug. 1984.

[20] L. K. Patton and B. D. Rigling
Phase retrieval for radar waveform optimization
IEEE Trans. Aerosp. Electron. Syst., vol. 48, no. 4, pp. 3287–3302, Oct. 2012.

[21] L. K. Patton and B. Rigling
Autocorrelation and modulus constraints in radar waveform optimization
In *Proc. Int. Waveform Diversity Des. Conf.*, Kissimmee, FL, USA, Feb. 2009, pp. 150–154.

[22] M. Kassab, M. Lesturgie, and J. Fiorina
Alternate projections technique for radar waveform design
In *Proc. Int. Radar Conf.*, Bordeaux, France, 2009, pp. 1–4.

[23] S. Blunt, M. Cook, J. Jakabosky, J. de Graaf, and E. Perrins
Polyphase-coded FM (PCFM) radar waveforms, part I: Implementation
IEEE Trans. Aerosp. Electron. Syst., vol. 50, no. 3, pp. 2218–2229, Jul. 2014.

[24] S. Blunt, J. Jakabosky, M. Cook, J. Stiles, S. Seguin, and E. Mokole
Polyphase-coded FM (PCFM) radar waveforms, part II: Optimization
IEEE Trans. Aerosp. Electron. Syst., vol. 50, no. 3, pp. 2230–2241, Jul. 2014.

[25] J. Jakabosky, S. D. Blunt, M. R. Cook, J. Stiles, and S. Seguin
Transmitter-in-the-loop optimization of physical radar emissions
In *Proc. IEEE Radar Conf.*, Atlanta, GA, USA, May 2012, pp. 0874–0879.

[26] Y. Lu, D. Peroulis, S. Mohammadi, and L. Katehi
A MEMS reconfigurable matching network
IEEE Microw. Wireless Compon. Lett., vol. 13, no. 10, pp. 437–439, Oct. 2003.

[27] T. Vaka-Heikkila and G. Rebeiz
A 4–18 GHz reconfigurable RF MEMS matching network for power amplifier applications
Int. J. RF Microw. Comput. Aided Eng., vol. 14, no. 4, pp. 356–372, Jul. 2004.

[28] N. Deve, A. Kouki, and V. Nerguizian
A compact size reconfigurable 1–3 GHz impedance tuner suitable for RF MEMS applications
In *Proc. 16th Int. Conf. Microelectron.*, Dec. 6–8, 2004, pp. 101–104.

[29] Y. Sun, J. Moritz, and X. Zhu
Adaptive impedance matching and antenna tuning for green software-defined and cognitive radio
In *Proc. 54th IEEE Int. Midwest Symp. Circuits Syst.*, 2011, pp. 1–4.

[30] Y. Sun
Evolutionary tuning method for automatic impedance matching in communication systems
In *Proc. IEEE Int. Conf. Electron., Circuits Syst.*, vol. 3, 1998, pp. 73–77.

[31] Y. Sun and W. K. Lau
Antenna impedance matching using genetic algorithms
In *Proc. IEE Conf. Antennas Propag.*, York, U.K., Aug. 1999, pp. 31–36.

[32] W. du Plessis and P. Abrie
Lumped impedance matching using a hybrid genetic algorithm
Microw. Opt. Technol. Lett., vol. 37, no. 3, pp. 201–212, May 2003.

[33] M. Fellows, C. Baylis, J. Martin, L. Cohen, and R. J. Marks II
Direct algorithm for the pareto load-pull optimization of power-added efficiency and adjacent-channel power ratio
IET Radar, Sonar Navig., vol. 8, no. 9, pp. 1280–1287, Dec. 2014.

[34] J. Barkate *et al.*
Fast, simultaneous optimization of power amplifier input power and load impedance for power-added efficiency and adjacent-channel power ratio using the power smith tube
IEEE Trans. Aerosp. Electron. Syst., vol. 52, no. 2, pp. 928–937, Apr. 2016.

[35] J. W. Bandler
Optimization methods for computer-aided design
IEEE Trans. Microw. Theory Techn., vol. 17, no. 8, pp. 533–552, Aug. 1969.

[36] A. Tsatsoulas, J. Barkate, C. Baylis, and R. J. Marks II
A simplex optimization technique for real-time, reconfigurable transmitter power amplifiers
In *Proc. IEEE MTT-S Int. Microw. Symp.*, San Francisco, CA, USA, 2016, pp. 1–4.

[37] J. Barkate, A. Tsatsoulas, C. Baylis, L. Cohen, and R. J. Marks II
Comparison of multidimensional circuit optimization techniques for real-time transmitter use
In *Proc. Texas Symp. Wireless Microw. Circuits Syst.*, Waco, TX, USA, Mar. 2016, pp. 1–7.

[38] Z. Hays *et al.*
Real-time amplifier optimization algorithm for adaptive radio using a tunable-varactor matching network
In *Proc. IEEE Radio Wireless Symp.*, Phoenix, AZ, USA, Jan. 2017, pp. 215–217.

[39] D. Eustice, C. Baylis, L. Cohen, and Marks II, R.J.
Effects of power amplifier nonlinearities on the radar ambiguity function
In *Proc. IEEE Radar Conf.*, Arlington, VA, USA, May 2015, pp. 1725–1729.

[40] C. Baylis *et al.*
Radar power amplifier circuit and waveform optimization for spectrally confined reconfigurable radar systems
In *Proc. IEEE Radar Conf.*, Ottawa, ON, Canada, 2013, pp. 1–4.